ELEMENTA
Science of the Anthropocene

Floerchinger, C, et al. 2021. Relative flux measurements of biogenic and natural gas-derived methane for seven U.S. cities. *Elem Sci Anth*, 9: 1. DOI: https://doi.org/10.1525/elementa.2021.000119

RESEARCH ARTICLE

Relative flux measurements of biogenic and natural gas-derived methane for seven U.S. cities

Cody Floerchinger[1,*], Paul B. Shepson[2,3], Kristian Hajny[2], Bruce C. Daube[1], Brian H. Stirm[4], Colm Sweeney[5], and Steven C. Wofsy[1,*]

Using the Purdue University Airborne Laboratory for Atmospheric Research, we measured concentrations of methane and ethane emanating from seven U.S. cities (New York, NY, Philadelphia, PA, Washington, D.C./Baltimore, MD, Boston, MA, Chicago, IL, Richmond, VA, and Indianapolis, IN), in order to determine (with a median 95% CI of roughly 7%) the fraction of methane emissions attributable to natural gas (Thermogenic Methane Emission Ratio [TMER]), for both summer and winter months. New methodology is introduced to compute inflow concentrations and to accurately define the spatial domain of the sampling region, using upwind measurements coupled with Lagrangian trajectory modeling. We show discrepancies in inventory-estimated TMER from cities when the sample domain is defined using political boundaries versus urban centers encircled by the flight track and highlight this as a potential source of error common to top-down studies. We found that methane emissions of natural gas were greater than winter biogenic emissions for all cities except Richmond, where multiple landfills dominate. Biogenic emissions increased in summer, but natural gas remained important or dominant (20%–80%). National inventories should be updated to reflect the dominance of natural gas emissions for urban environments and to account for seasonal increases in biogenic methane in summer.

Keywords: Urban methane, Airborne greenhouse gas measurements, Methane emissions

1. Introduction

Methane (CH_4) is a potent greenhouse gas with contemporary concentrations today almost three times greater than in preindustrial times. Anthropogenic emissions of CH_4 have been studied from a wide range of sources, including agriculture, landfills, and oil and gas production, transportation, and processing (Börjesson and Svensson, 1997; Marchese et al., 2015; Roscioli et al., 2015; Subramanian et al., 2015; Eilerman et al., 2016). Emissions of CH_4 from cities has been a topic of increasing interest in recent literature (McKain et al., 2015; Lamb et al., 2016; Plant et al., 2019). The underlying sources of urban emissions remain poorly understood (Alvarez et al., 2018) because they are spatially diffuse and arise from diverse source types including landfills, wastewater treatment street-level sewage leaks, natural gas leaks from distribution or within individual homes, appliances, and so on. Bottom-up inventories have been shown to underestimate the total magnitude, source distributions, and seasonal variability of CH_4 emissions within urban domains (Cui et al., 2015; McKain et al., 2015; Lamb et al., 2016).

Here we present aircraft measurements to determine a fundamental attribute of urban CH_4 emissions, the partitioning between biogenic (e.g., from landfills, wetlands, or sewers) and thermogenic CH_4 emissions (natural gas). This characterization provides a strong constraint for understanding the emission sources and designing mitigation pathways. We report airborne measurements of CH_4 and ethane (C_2H_6; a component of natural gas) from seven urban areas representative of eastern and midwestern U.S. cities: Indianapolis, IN, Chicago, IL, Washington, DC, and Baltimore, MD, Philadelphia, PA, New York, NY, Richmond, VA, and Boston, MA. We use measurements of the C_2H_6:CH_4 ratio to estimate the fraction of urban CH_4 emissions that can be attributed to natural gas, with the rest (not associated with C_2H_6) attributed to biogenic sources. Our data show how partitioning of CH_4 emissions changes by season and is dependent on the urban setting. Our analysis also contributes methodological developments to help precisely define the measurement domain sampled by the

[1] Department of Earth and Planetary Sciences, Harvard University, Cambridge, MA, USA
[2] Department of Chemistry, Purdue University, West Lafayette, IN, USA
[3] School of Marine and Atmospheric Sciences, Stony Brook University, Stony Brook, NY, USA
[4] School of Aviation & Transportation Technology, Polytechnic Institute, Purdue University, West Lafayette, IN, USA
[5] Global Monitoring Division, Earth System Research Laboratory, National Oceanic and Atmospheric Administration, Boulder, CO, USA

* Corresponding authors:
Emails: codyfloerchinger@g.harvard.edu; wofsy@g.harvard.edu

aircraft observations, as well as the background inflow concentrations entering the region. We also compare our results to those from an established network of tower measurements of CH_4 and carbon dioxide (CO_2) in Boston, MA, to test our methodology.

Measurements of C_2H_6 and CH_4 in the atmosphere enable us to partition biogenic and thermogenic emissions because biogenic CH_4 is not co-emitted with C_2H_6. Thermogenic processing of organic carbon at extreme temperatures and pressures (Kidnay et al., 2011) produces CH_4 along with higher hydrocarbons (C2+). Only a portion of the higher hydrocarbons is extracted as feedstock during the processing of natural gas before it enters the market. Thus, natural gas distributed throughout a city is composed of a mixture of hydrocarbons, the two most prevalent being CH_4 ($\approx$ 95%) and C_2H_6 ($\approx$3%). The C_2H_6: CH_4 ratios are somewhat variable, depending on market conditions and origin of the natural gas, but ratios at transmission stations are regularly monitored and reported to the public continuously as "gas quality" data. It is commonly accepted that natural gas is the only significant source of urban C_2H_6 in most large cities across the United States, and other studies have leveraged these tracer-tracer ratios in a similar manner (McKain et al., 2015; Lamb et al., 2016; Plant et al., 2019).

Maasakkers et al. (2016) presented a spatially resolved version of the Environmental Protection Agency CH_4 inventory for the Continental United States (Gridded EPA inventory: GEPA), reporting anthropogenic CH_4 emissions from 22 source sectors of both biogenic and thermogenic origin. GEPA estimates the most significant biogenic sectors in the cities studied here are municipal and industrial landfills and wastewater treatment plants (WWTP). GEPA also estimates that the thermogenic (natural gas) emission sources in the study cities are primarily natural gas transportation and distribution infrastructure. End user emissions were excluded from the GEPA inventory because only a small number of case studies have been reported for "post-meter" sources such as appliances, leaks in houses, commercial equipment, and so on, and their aggregated contributions and urban spatial distributions are unknown (Merrin and Francisco, 2019; Saint-Vincent and Pekney, 2020).

An early study of C_2H_6: CH_4 ratios in eastern Massachusetts (McKain et al., 2015) showed that the "Thermogenic Methane Emissions Ratio" (TMER, $\frac{\mathrm{Flux}CH_4(\mathrm{Thermogenic})}{\mathrm{Flux}CH_4(\mathrm{Total})}$) exhibited significant seasonal variations, with more biogenic emissions in summer. There were no statistically significant seasonal changes detected in thermogenic emissions. Our objectives in this study are to quantify the thermogenic fraction of urban CH_4 emissions in seven cities, then use our results to assess the accuracy of the source attribution in available inventories. Our observations also allow us to assess whether summer increases in the fractional biogenic emission component are significant in other urban regions. We report here that TMER declines in summer in four of the six cities that were sampled in both seasons. Our observations, coupled to the results from McKain et al. (2015), suggest that higher biogenic emissions are typical in the summer season.

2. Methods

2.1. Sampling platform

Campaigns were flown in August/September 2017 and March 2018 on board the Purdue University Airborne Laboratory for Atmospheric Research, a fully instrumented Beechcraft 76 Duchess with a long history of making atmospheric trace gas measurements. The flight tracks are shown in **Figure 1** for each season. The aircraft was outfitted with a Picarro Cavity Ring Down Spectrometer (model G2301-m) measuring CO_2, CH_4, and H_2O, and a direct absorption C_2H_6 analyzer designed by Aerodyne Research Inc. and reengineered at Harvard University to improve stability under flight conditions (Crosson, 2008; Yacovitch et al., 2014). Typical 1s precision in flight was roughly 100 ppb (ppb; $\frac{10^{-9}\mathrm{mol}}{\mathrm{mol_{air}}}$), 1 ppb, and 50 ppt (ppt; $\frac{10^{-12}\mathrm{mol}}{\mathrm{mol_{air}}}$) for CO_2, CH_4, and C_2H_6 respectively. For these flights, the gas phase H_2O measurement was not calibrated, though it is included in the data set for diagnostic purposes. A Best Air Turbulence Probe (BAT Probe) provided accurate and fast (50 Hz) 3-component wind speed and direction measurements (Crawford and Dobosy, 1992; Garman et al., 2006) on a subset of the flights. The CH_4, CO_2, and C_2H_6 measurements were calibrated in flight by sampling from high pressure standard gases traceable to World Meteorological Organization/Global Atmosphere Watch calibration scales (CH_4: X2004, CO_2: X2007). The C_2H_6 instrument was also corrected for instrument background drift with periodic in-flight injections of hydrocarbon free zero air (roughly 30s each); these zero injections are removed from the ambient data and filled by linear interpolation. More information about the instrument performance, calibration source gases, and calibration practices of the ALAR gas phase instruments can be found in Section 1 of the Supplemental Information (SI). Because the ALAR deployment did not sample Philadelphia, PA, in winter, we use data collected during the National Oceanic and Atmospheric Administration (NOAA) East Coast Outflow (ECO) Campaign on April 26, 2018, in our winter analysis for that city. ECO flights were deployed using a NOAA Twin Otter, with C_2H_6 measurements using the same Harvard instrument and a comparable Picarro spectrometer was used to measure CH_4 (see Plant et al., 2019).

2.2. Experimental design

All flights (except one) carried out transects both upwind and downwind of the urban areas, sampling both the inflow and urban-influenced outflow. Flight days and sampling times were chosen based on forecast meteorology such that wind speed and direction was fairly constant throughout the flight, the Planetary Boundary Layer (PBL) was well developed to ensure steady transport across the sample domain, and that the aircraft was able to fly in the PBL in order to sample well mixed urban sources. Sampling transects usually occurred between 300 and 600 m above ground level.

Flights were designed to sample the outflow from the urban core of each city, as defined by the size and shape of the downwind plume. Downwind transects were selected for analysis from each flight based on the measured mixing ratio enhancements and the domain sampled by that

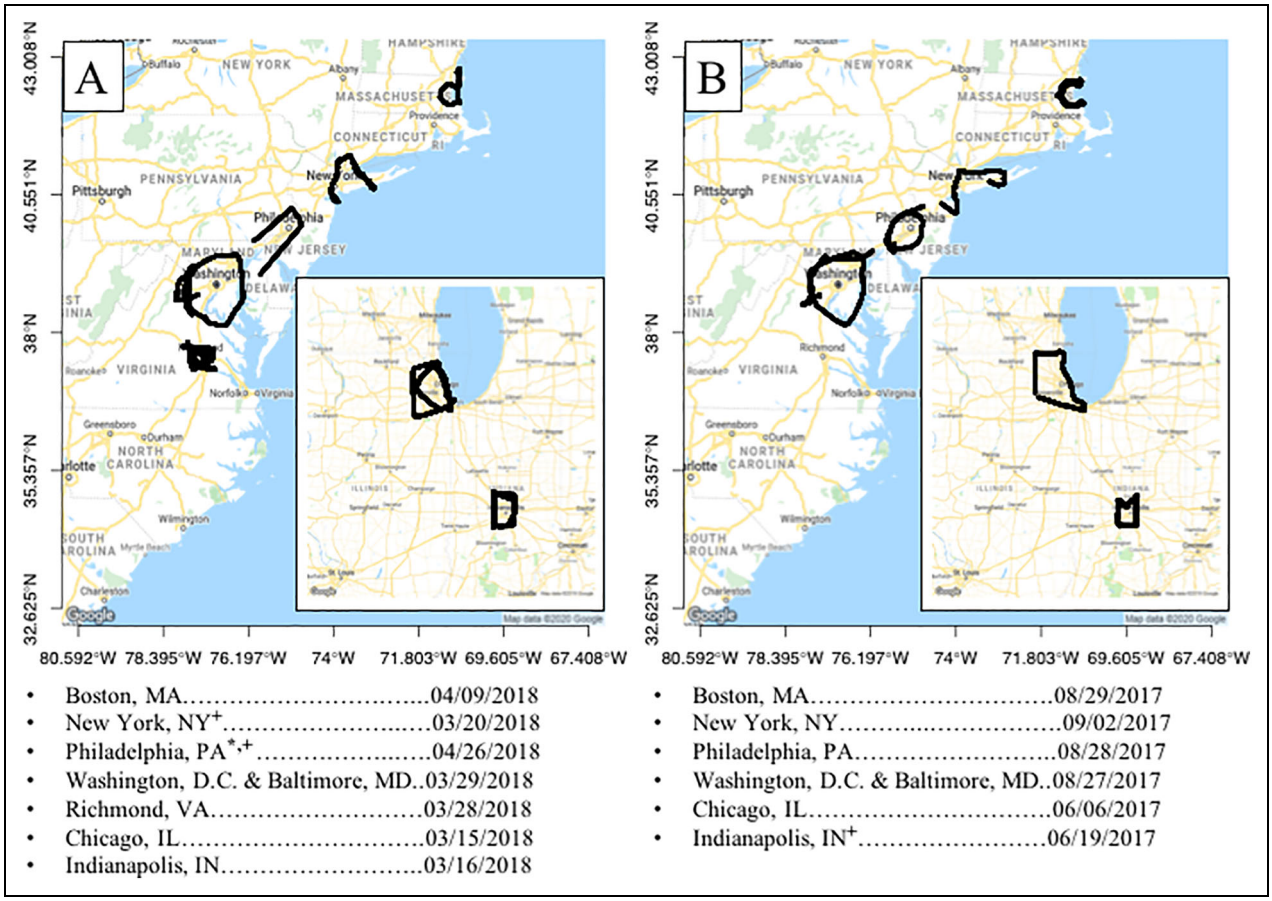

Figure 1. Campaign flight tracks. Panel A shows the flight tracks of the winter flights in March and April 2018. Panel B shows the flight tracks of the summer flights in August and September 2017. The inset panels in each side show flights in Indianapolis, IN, and Chicago, IL. +Indicates that the uncertainty for this flight may be underestimated due to suboptimal measurements of the inflow conditions. *Indicates flight was a part of the NOAA ECO campaign. DOI: https://doi.org/10.1525/elementa.2021.000119.f1

particular transect according to our analysis of transport such that cities that were sampled in both seasons, but for different meteorological conditions with downwind transects in multiple locations (Boston, MA, August 29, 2017), could be readily and effectively compared. In the case of the winter flight in Indianapolis where there were three identical transects flown, the transects were analyzed separately and the results were bootstrapped to obtain a single TMER for that flight (Section 6 of the SI). **Figure 2** shows an example flight from Indianapolis, IN, on March 16, 2018, with prevailing winds from the east, with the upwind and downwind mixing ratio enhancements readily seen by the color scale.

2.3. Thermogenic methane emission ratio determination

In order to calculate the ratios of biogenic and thermogenic CH_4 flux for a particular city (TMER, $\frac{\mathrm{FluxCH_4(Thermogenic)}}{\mathrm{FluxCH_4(Total)}}$), downwind CH_4 and C_2H_6 mixing ratio enhancements are computed by subtracting background values from the downwind measurements and integrating along the downwind flight track. Equation 1 is then used to solve for the TMER from each domain by computing the flux of CH_4 and C_2H_6 through a plane perpendicular to the ground at the height of the aircraft taking into account the mole fraction enhancements observed at the aircraft and the associated wind speed and direction. Our method assumes that thermogenic emissions of CH_4 from an urban domain can be approximated using a single ethane to methane emission ratio (EMER, $\frac{\mathrm{moles_{C_2H_6}}}{\mathrm{moles_{CH_4}}}$) published by pipeline companies in the mandated gas quality portion of their public informational postings (McKain et al., 2015; Smith et al., 2015; Lamb et al., 2016; Plant et al., 2019). To account for error associated with the EMER from either onsite measurement uncertainty at the reporting stations or the variable residence time of natural gas within the network, we used the mean +/− 1 standard deviation ($\epsilon_{\mathrm{EMER}} = \pm 1\sigma_{10\mathrm{day}}$) for all gas quality measurements reported in the 10 days prior to the measurement date. A detailed description of the data sources and determination of the EMER for each city is included in Section 2 of the SI.

$$\mathrm{TMER} = \frac{\int (\cos(\theta) * (\mathrm{C_2H_{6Downwind}} - \mathrm{C_2H_{6Inflow}}) * U)}{\int (\cos(\theta) * (\mathrm{CH_{4Downwind}} - \mathrm{CH_{4Inflow}}) * U)} * \mathrm{EMER}_{\mathrm{pipeline}}^{-1} + \epsilon_{\mathrm{transport}} + \epsilon_{\mathrm{EMER}} \quad (1)$$

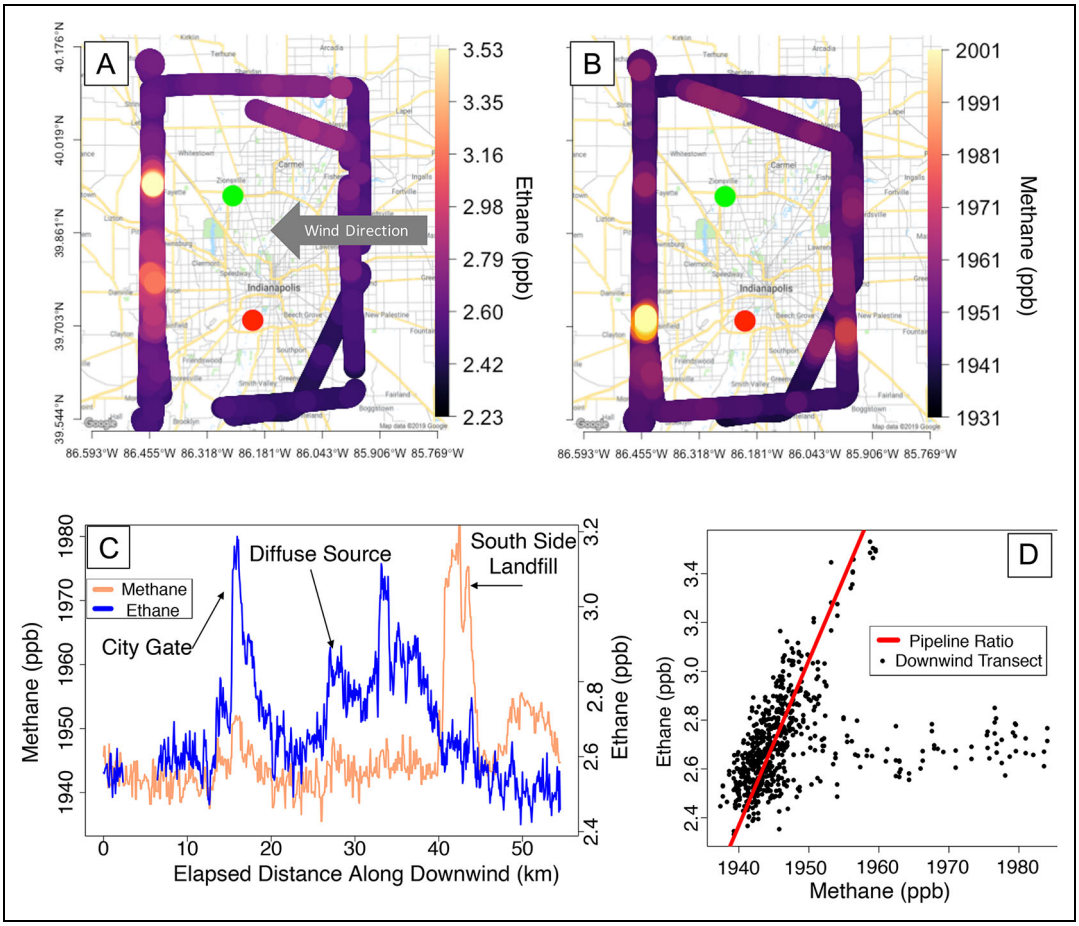

Figure 2. Example mixing ratio data from Indianapolis, IN. (A) and (B) CH_4 and C_2H_6 are plotted as a function of aircraft location. The green and red dots show the Zionsville City Gate and the South Side Landfill respectively. The X and Y axis of Panels A and B represent degrees Longitude and Latitude. (C) Example downwind time series, flying north to south, of CH_4 and C_2H_6 data from this flight with the time series signatures of three significant sources labeled. (D) Scatter plot of the downwind enhancement of CH_4 and C_2H_6 with the reported pipeline ratio of C_2H_6: CH_4 (0.063) plotted in red. DOI: https://doi.org/10.1525/elementa.2021.000119.f2

Equation 1: Computation of the Thermogenic Methane Emission Ratio (TMER) Individual terms are defined in the list below as:

- $\cos\theta$: nonorthogonality flight track correction factor
- $(X)_{\text{Downwind}}$: Downwind enhancement of CH_4 and C_2H_6
- $(X)_{\text{Inflow}}$: The modeled inflow concentration, either MDI or linear background
- U: The North American Mesoscale Forecast System hourly 12 km (NAMS-12 km) wind speed.
- $\text{EMER}_{\text{pipeline}}$: The reported Ethane: Methane Emission Ratio of the distribution system
- $\epsilon_{\text{transport}}$: Error term associated with transport when determining the MDI
- ϵ_{EMER}: Error term associated with the variability in the reported EMER

2.4. Computing the model derived inflow (MDI) and meteorological parameters for the TMER calculation

For 8 (of 13) flights with the most complex inflow patterns, we used an atmospheric transport model and measurements along the upwind transect measured during each flight to determine an MDI or effective inflow concentrations that can be subtracted from each mixing ratio observation in the downwind transect, to compute downwind enhancements due to urban emissions. To calculate the MDI for each flight, we use multi-particle back trajectories from the Stochastic Time Inverted Lagrangian Transport Model (STILT; Fasoli et al., 2018). The STILT model is a Lagrangian atmospheric transport model that can be run backward in time to statistically represent atmospheric dispersion and transport before an air mass reaches a particular point in time and space (the receptor).

Ensembles of STILT runs were executed from receptor points distributed along each downwind flight track, spaced 10s apart. For each receptor, 500 particles were released and advected backward in time for 10 h, ensuring all particles were allowed sufficient time to exit the urban

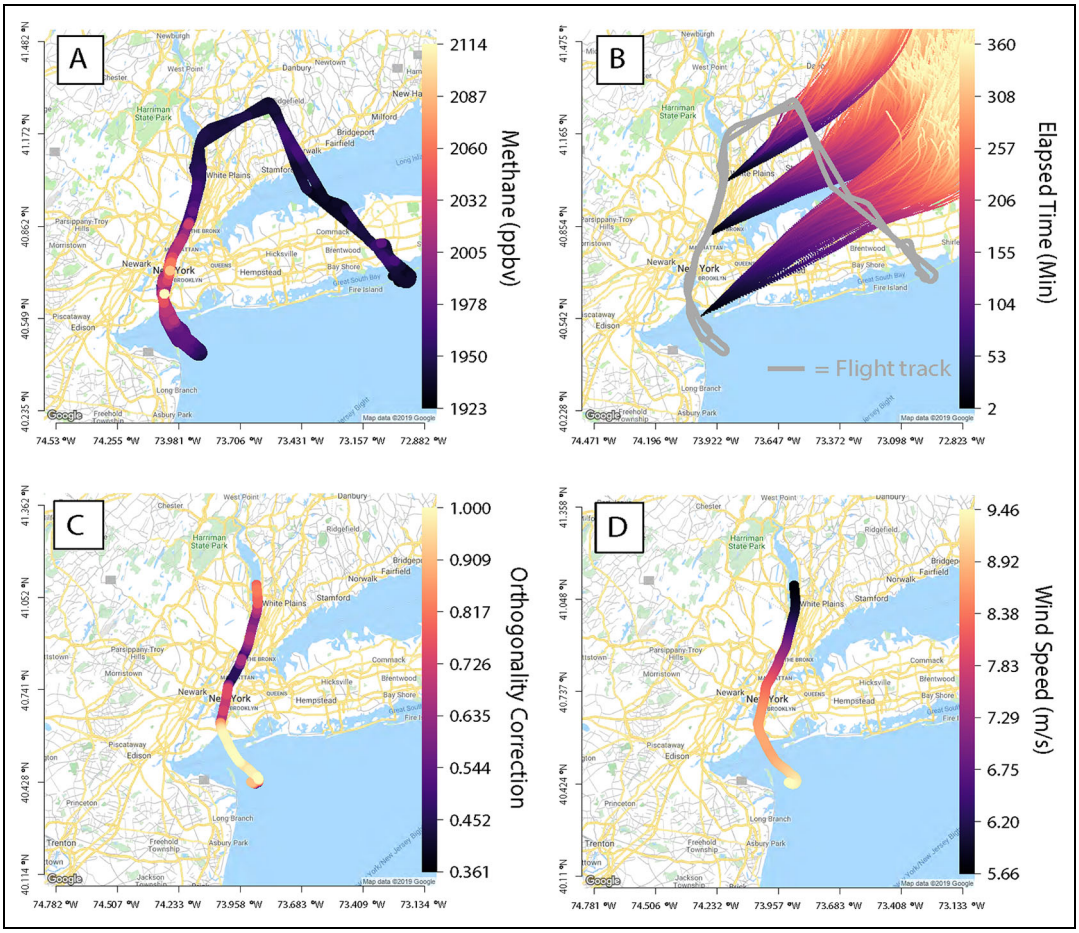

Figure 3. Example of a STILT particle release. Panel A shows the measured CH_4 mixing ratio along the flight track. Panel B shows the particles as they are transported through the STILT model from three example receptors; particles are colored as a function of the time since their release. Panel C shows the nonorthogonality factor computed from the North American Mesoscale Forecast System hourly 12 km wind direction. Panel D shows the horizontal wind speed (U). The X and Y axis of Panels A, B, C, and D represent degrees Longitude and Latitude. DOI: https://doi.org/10.1525/elementa.2021.000119.f3

domain under study. Example STILT releases from three receptors along the flight track are shown in **Figure 3**. The inflow concentration values for each downwind receptor were determined from the measured values at each point where a STILT particle crossed the upwind transect. The STILT model was driven by the NAMS-12 km product as archived at the NOAA Air Resources Laboratory (ARL; Stein et al., 2015).

For each receptor point, the inflow value was calculated as the mean of 500 upwind mole fraction estimates inferred from the back trajectories of the Lagrangian particles. The MDI was then smoothed along the downwind flight track with a penalized spline to account for the spatial resolution of the STILT receptors. The enhancements were then calculated by subtracting the smoothed MDI from the downwind measurements.

The errors in the transport simulations were taken into account when computing the overall uncertainty of the MDI (Section 3 of the SI). The STILT model can incorporate optional parameters to account for spatio-temporal error and autocorrelation in the horizontal and vertical advection parameters of the input meteorological model as well as error in the model estimate of the height of the planetary boundary layer (Fasoli et al., 2018). Lin and Gerbig (2005) describe how STILT increases the magnitude of the stochastic transport component applied to particle transport to statistically represent the impact of meteorological error on the resulting spatial distribution of the modeled particles (Lin and Gerbig, 2005). The STILT model then creates a second distribution of particles that statistically represents the transport error. The difference between total errors in MDI, calculated using the "error-added" particle distributions, and the MDI calculated using the original particle distributions, approximates the effect of the meteorological error on the MDI (Equation 2).

$$\epsilon^2_{\text{transport}} = \sigma^2_{\text{w/error}} - \sigma^2 \quad (2)$$

Equation 2: Determination of transport error when computing the MDI Individual terms are defined in the list below as:

- $\epsilon^2_{\text{transport}}$: The actual variance of the transport error due to meteorological uncertainty
- $\sigma^2_{\text{w/error}}$: The variance of the transport error of the MDI with added meteorological error

- σ^2: The variance of the transport error of the MDI without added meteorological error

For 3 of the 13 flights presented (August 29, 2017, Boston, MA, June 6, 2017, Chicago, IL, September 2, 2017, New York, NY), we were able to measure the downwind enhancement with particularly stable upwind concentrations. These flights occurred in the presence of an onshore wind, and operational and aircraft safety constraints did not always allow the plane to fly over the water in order to observe upwind concentrations. Hence, a complete upwind fetch was not always flown. In these cases, the downwind enhancement was calculated using conventional methodology by subtracting a background that was computed by linearly interpolating the average background values observed on each side of the plume (Heimburger et al., 2017). For these flights in New York, NY, and Boston, MA, the wind vector was a consistent onshore fetch from the Atlantic Ocean. For the flight in Chicago, IL, there was a consistent onshore fetch from Lake Michigan. We are confident that for these three flights, there were no upwind sources of CH_4 or C_2H_6 significantly contributing to the downwind enhancement.

For two flights (April 26, 2018, Philadelphia, PA, and June 19, 2017, Indianapolis, IN), the aircraft did not accomplish an upwind flight transect that was suitable to compute an MDI, and the dominant airflow was not from regions where we can *definitively* say there were no sources of CH_4 or C_2H_6 upwind. The background was calculated using the interpolation method described above (Heimburger et al., 2017). In these cases, the errors associated with the TMER may be larger than included in our error estimates. We believe that the added uncertainty during these two flights is not large enough to affect our conclusions; these two flights are discussed in detail in Section 6 of the SI and are denoted with a "+" in **Figure 1**.

The TMER is the ratio of CH_4 and C_2H_6 fluxes across a hypothetical curtain traced by the flight track (Equation 1). To compute the ratio of the CH_4 and C_2H_6 fluxes transported through this curtain, we correct for the nonorthogonality of the aircraft heading with respect to the mean wind direction along the flight transect. We calculate an angle (Θ) at 10s intervals along the downwind transect, where Θ is the angular deviation from normal of two vectors representing the direction of flight and the wind direction at the aircraft. The direction of flight is based on the direction of motion of the aircraft in time, and the mean wind direction is derived from the NAMS-12 km product at the point in time and space where the aircraft flew. The horizontal wind speed (U) (Figure 3D) was also determined from the NAMS-12 km model. The meteorological factor is then calculated $(\cos(\Theta) * U)$ and applied to each point along the downwind transect to obtain the flux through the curtain at that point (Figure 3C).

In order to assess the magnitude of the instantaneous error of the NAMS-12 km meteorology, a model-data comparison was done for three flights using the wind speed and direction measured by the onboard BAT Probe and values from NAMS-12 km. BAT Probe measurements were averaged to 45 s, and the temporally corresponding values were extracted from the NAMS-12 km meteorology. These analyses show a nominal average wind direction error of roughly 11° and an average wind speed error of roughly 1.5 m/s. This comparison is described in further detail in Section S3 of the SI.

2.5. Defining the emission domain influencing the downwind plume

The STILT model was originally developed to understand the influence of surface sources on enhancements observed at the point of measurement (Lin et al., 2003) by generating a sensitivity matrix (footprint) for a specific receptor to solve for the geospatial upstream surface influence ($\mathrm{ppm} * (\frac{\mu\mathrm{mol}}{\mathrm{m^2 s}})^{-1}$) (Fasoli et al., 2018). For this study, the STILT model was run at 10s intervals along the downwind flight track and footprints were generated at a spatial resolution of $0.025^\circ \times 0.025^\circ$ (roughly 6.5 $\mathrm{km^2}$). The footprint domains were defined so the target city and immediately outlying areas could be fully enclosed within the domain and are shown in Section 5 of the SI. The spatially resolved sensitivity of the ratio of the calculated flux at the curtain to the surface emissions can be calculated by Equation 3. We represent this flux sensitivity graphically by multiplying each downwind footprint by the meteorological variables in the flux calculation $(\cos(\Theta) * U)$, then summing the set of footprints for the total downwind flight transect and normalizing them from 0 to 1. The result allows us to verify that the domains were sampled in a way that did not bias the calculated flux ratio to a small area of the urban domain due to either meteorological conditions or inconsistencies in the flight profile.

$$\delta\mathrm{Flux}_{xy} = \int \left(U * \cos(\theta) \left(\int (\mathrm{Foot}_{xy} * \mathrm{Emiss}_{xy} * dx * dy * dt) \right) \right) * dx * dy \tag{3}$$

Equation 3: Sensitivity of measurement to a specific grid box within the domain. Individual terms are defined in the list below as:

- $\delta\mathrm{Flux}_{xy}$: The sensitivity of the receptor to the flux at grid box xy
- U: The NAMS-12 km wind speed
- $\cos(\theta)$: nonorthogonality flight track correction factor
- Foot_{xy}: The footprint value at grid box xy
- Emiss_{xy}: The emissions at grid box xy

2.6. Calculation of regional inventories emission rates

We compared to published inventories in order to contextualize our results and to evaluate the current understanding of greenhouse gas emissions from urban areas. For CH_4 emissions, we used the gridded EPA CH_4 inventory (Maasakkers et al., 2016). GEPA is a multi-sector CH_4

inventory with 0.1° × 0.1° spatial resolution. Of the 22 sectors reported in the inventory, we identified 12 as being of thermogenic origin and having the potential for C_2H_6 co-emissions as shown in Section 5 of the SI. In order to calculate the inventory flux of CH_4 from each urban domain, GEPA was reprojected onto a Universal Transverse Mercator coordinate system so the total flux could be calculated using equal area grid boxes. After reprojection, the GEPA inventory was summed for each city. To investigate the sensitivity of our analysis to the prescribed domain boundaries, we summed the inventory in two ways (1) by subdividing the inventory based on the urbanized area boundaries defined by the U.S. Census Bureau in the Topologically Integrated Geographic Encoding and Referencing (TIGER) database and (2) by subdividing the inventory based on the flight tracks to compute the inventory emissions from the actual measured area (primarily the urban cores of each city). In order to understand how representative GEPA was to another large scale CH_4 inventory, the TMER for each city was also compared to the TMER calculated using EDGAR v 4.3.2. This comparison is shown in Section 6 of the SI.

Because CO_2 and CH_4 measurements are much more common than C_2H_6 measurements, we used the CO_2: CH4 ratio to assess our methodology against existing data. We used the Anthropogenic Carbon Emission System (ACES) CO_2 emission inventory (Gately and Hutyra, 2017) for additional evaluation of our inventory framework. ACES is a 1 km × 1 km anthropogenic CO_2 emissions inventory with hourly resolution compiled for 2013 and 2014. For this study, we used the average ACES emissions across all days in April 2014 from 18:00:00 to 22:00:00UTC and used that to calculate the CO_2 flux of each urban domain. Like GEPA, ACES was masked and summed based on the TIGER boundaries and the flight domains in order to determine the respective hourly emission rates of CO_2 from each urban domain sampled by the aircraft and to determine how susceptible total emission estimates are to the definition of the domain.

2.7. Comparison to ground network data

We compared the ratio of integrated CH_4 and CO_2 enhancements computed from our flights to data from the Harvard–Boston University Greenhouse Gas Network in the city of Boston, MA, as an additional evaluation of our methodology. The Harvard Copley site samples CH_4 and CO_2 at a height of 215 m and is located in the core city of Boston, MA (for a complete description of the site, refer to Sargent et al., 2018). Tower time series data for the month of April were subselected to include only daytime data between the hours of 12 p.m. and 5 p.m. local to ensure sampling when the tower inlet was within the daytime planetary boundary layer and to ensure that the observed enhancements would be comparable to the daytime aircraft flight. A standard major axis regression was then computed using the calibrated mixing ratios to determine a characteristic ratio between CO_2 and CH_4 for the Boston urban Core. Enhancement ratios using CO_2 from the Copley site were compared for winter, but not for summer, due to difficulty in resolving effects of CO_2 uptake by the summer biosphere (Briber et al., 2013; McKain et al., 2015; Sargent et al., 2018). We also present a comparison to tower measurements of TMER made in Indianapolis by the INFLUX project (Lamb et al., 2016). These comparisons further highlight the need for accurate representations of the sample domain, especially when attempting to compare multiple measurements of the same urban area.

3. Results

3.1. MDI and ground influence

Figure 4B shows a typical MDI for a downwind plume, as calculated for the winter flight on April 9, 2018, over the urban core of Boston, MA. Structure in the MDI is a function of variable mixing ratios observed in the upwind transect and their transport across the domain into the downwind measurement, as simulated by the STILT model. Results from the comparison of horizontal winds from NAMS-12 km meteorology to the horizontal winds from the ALAR BAT probe measurement suggest that the error in the NAMS-12 km model was small and well accounted for in the parameters adapted from Lin and Gerbig (2005), and Gerbig et al. (2008). We computed a mean absolute direction error in the NAMS-12 km meteorology of only 11.2 (degrees) [10.6, 11.9] ($\pm 1\sigma$). The mean wind speed difference showed NAMS-12 km to be 1.5 (m/s) [1.33, 1.68] (($\pm 1\sigma$) faster than the winds measured by the BAT probe with mean measured wind speeds averaging 7.56 (m/s). These results are further described in Section 4 of the SI. Subtraction of the MDI from the downwind measurement leaves the concentration enhancement due to emissions in the urban domain between upwind and downwind flight transects, enabling us to compute the TMER.

Domain sensitivity maps illustrate the measurement domain sampled by each flight and depict the relative sensitivity of the TMER to emissions in each grid box within the domain. **Figure 4C** shows an influence map for the April 9, 2018, flight. As expected, the grid boxes closer to the aircraft more heavily influence the downwind enhancement used to compute the TMER. Domain sensitivity maps for other flights are shown in Section 5 of the SI (Figures S8–S21) and identify the domain sampled by the aircraft for all cities. The U.S. Census Bureau TIGER borders are overlaid on the influence maps in green and show that, in most cases, the aircraft sampled only the urban core of each city. Notably, the measurement domains are not well represented by political boundaries and must be further defined with tools such as meteorological models and footprint modeling as done here. Domain sensitivity maps for the remaining flights support the assertion that similar urban core domains were sampled by flights in various meteorological conditions and can be compared in our analysis (i.e., winter and summer).

3.2. Thermogenic methane emission fractions

We observed good agreement throughout this study between published EMERs and the slope of CH_4 and C_2H_6 enhancements at those points in the track where we expect the sources to be predominantly natural gas, such as for the city gate sampling shown in Figure 2.

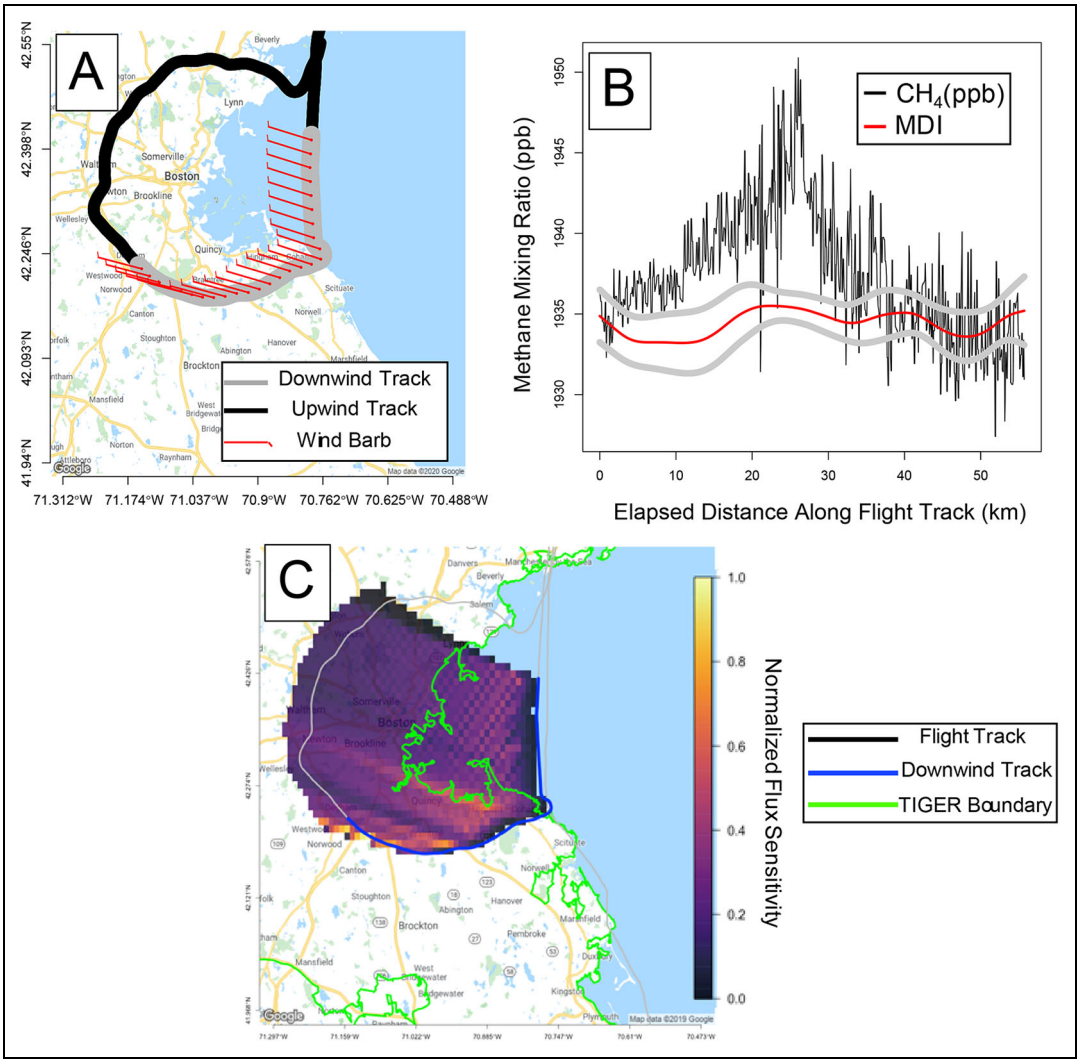

Figure 4. Example MDI and normalized flux sensitivity. Panel A shows the upwind and downwind flight tracks for the flight on April 9, 2018. Panel B shows the CH_4 mixing ratio observed in the downwind transect along with the calculated MDI (MDI uncertainty shown in gray). Panel C shows the normalized sensitivity of the calculated flux ratio to emissions on the ground. The borders of the Topologically Integrated Geographic Encoding and Referencing Domain are overlaid in Panel C. The X and Y axis of Panels A and C represent degrees Longitude and Latitude. DOI: https://doi.org/10.1525/elementa.2021.000119.f4

Tracer-tracer plots comparing the downwind measurements of CH_4 and C_2H_6 for each flight to the EMER obtained from the pipeline companies (e.g. Figure 2D) are shown in Section 9 of the SI (Figure S26). Figure 2D shows an example tracer-tracer plot observed downwind of Indianapolis, IN, where biogenic sources are a significant fraction of the city's total CH_4 emissions. The CH_4 enhancements that we attributed to emissions of natural gas are clearly separated in the time series from the biological landfill point source, and the slope of the enhancements agrees well with the published EMER (Figure 2D). The time series in Figure 2C shows three distinct sources that can be easily identified: the South Side Landfill (biogenic) and the City-Gate in Zionsville. Outside of those two easily distinguishable peaks in the time-series, our method is not able to attribute other enhancements to specific point sources, and thus, we refer to the rest of the urban plume as diffuse emission, likely from the natural gas distribution infrastructure, post-meter emissions, and other potential methane sources that may be collocated. Our estimate of the uncertainty in the EMER from the pipeline informational postings is discussed in Section 2 of the SI.

The calculated TMER values for each urban domain (Equation 1) are shown in **Figure 5.** In winter, the TMERs ranged from 0.32 for Richmond, VA, to 1 for New York, NY. Uncertainties in the TMER vary from very tight, for example, 0.815 (+0.004/–0.006) observed during a flight over New York, NY, on September 2, 2017, to significant uncertainty, for example, 0.384 (+1.23/–0.13) observed during a flight over Philadelphia, PA, on August 28, 2017. The differences in the calculated relative uncertainties are a function of the complexity of upwind source emissions, which result in increased uncertainty in the calculated MDI, as described in detail in Section 3 of the SI.

The TMER values measured in four of six cities showed statistically significant seasonal differences. The Boston

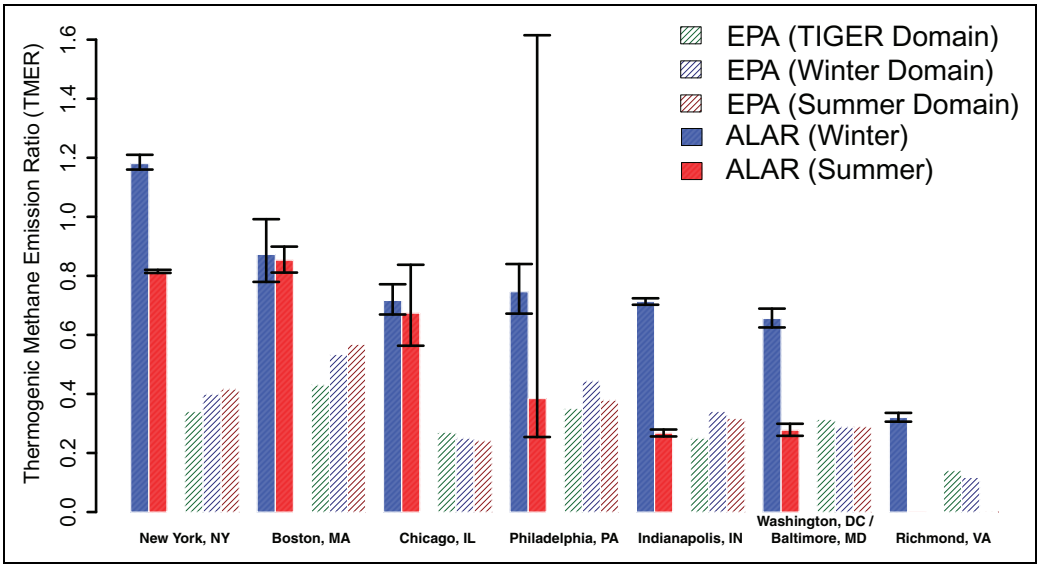

Figure 5. Thermogenic Methane Emission Ratio results for seven cities. Aircraft Thermogenic Methane Emission Ratio results for summer (red) and winter (blue) are compared to the GEPA inventory subset using the U.S. Census Bureau Topologically Integrated Geographic Encoding and Referencing Boundaries (green) and then subset based on the domain encircled by the aircraft (blue for winter flights and red for summer flights). DOI: https://doi.org/10.1525/elementa.2021.000119.f5

urban core did not show significant biogenic increase in summer compared to winter. McKain et al. (2015) reported a modest seasonality, with greater biogenic emissions in the spring/summer. Our flights sampled the urban core of the city (generally East of the I95 ring road), whereas the inverse model in the McKain study sampled CH_4 emissions from a much larger domain extending to the west. It is likely that the outlying rural and forest areas included in the McKain domain were the source of the seasonal increase of biogenic emissions observed in the Boston regional network in spring/summer.

Inventory estimates of TMER from the 12 thermogenic sectors in the GEPA inventory are shown **Figure 5.** Two subsets of the GEPA estimates are shown: a subset based on the TIGER boundaries drawn by the U.S. Census Bureau (Plant et al., 2019) and a subset for each flight with the domain defined as the area encircled by the aircraft. The TMER predicted by GEPA can vary by 15%–30% (up to 0.13 $\frac{\mathrm{FluxCH_4(Thermogenic)}}{\mathrm{FluxCH_4(Total)}}$) based on whether or not the inventory is subsampled using the domain bound by the sampling flight track or the U.S. Census Bureau's political boundaries. All of the inventory estimates of TMER were significantly lower than those measured by the aircraft in winter, and likewise three of the six cities measured in summer, regardless of inventory subset. GEPA estimated TMER from each city (except Boston, MA) to be less than 0.50, but values this low were observed by the aircraft on only 4 of 13 flights (winter: Richmond, VA, only; summer: Washington, DC/Baltimore, MD, Philadelphia, PA, Indianapolis, IN).

3.3. CO_2: CH_4 comparison to ground data

Since CO_2 emission inventories are based on reliable proxies (e.g., traffic data, building maps, power plant locations, and reported emissions; Sargent et al., 2018) not available for CH_4 emission inventories, accurate determination of the CO_2: CH_4 ratio can aid in the assessment of the urban CH_4 sources and source strengths (Plant et al., 2019). **Figure 6** shows the ratio of CO_2: CH_4 enhancement from each city measured during the winter flights compared to the ratio of ACES CO_2 emissions and the GEPA CH_4 emissions. Both inventories were subsampled using two domains for each flight: the U.S. Census Bureau TIGER boundaries and the urbanized core encircled by each flight. Every domain showed a larger CO_2: CH_4 inventory estimate when the flight domains were used to subsample the inventories as opposed to the TIGER boundaries, with the average effect being a difference in the CO_2: CH_4 ratio of 13.4%.

The ratio of CO_2: CH_4 enhancements measured at the Copley site in the Boston Urban Greenhouse Gas Network was 287 (+27/−22) mol CO_2: CH_4 ($r^2 = 0.84$, MA regression), in close agreement with the aircraft data (240 (+26/−12) $\frac{\mathrm{molCO_2}}{\mathrm{molCH_4}}$), using data from the April 2018 ALAR flight (**Figure 7**). This comparison to independent determination of TMER tests our methodologies, and the good agreement supports our flux ratio sampling method.

4. Discussion

4.1. Measurement and estimation of TMER

Determination of TMER, like inverse analysis of emissions, depends sensitively on the concentrations inferred in inflowing air (Karion et al., 2015; Heimburger et al., 2017; Bares et al., 2018). A simple method used previously draws a straight line between plume edge concentrations, suitable in specific settings where the target region is isolated, with a clean upwind fetch. This approach does not account for inflow effects of inhomogeneous concentrations entering the target region from the upwind boundary, as commonly found along the East Coast Corridor of the United States.

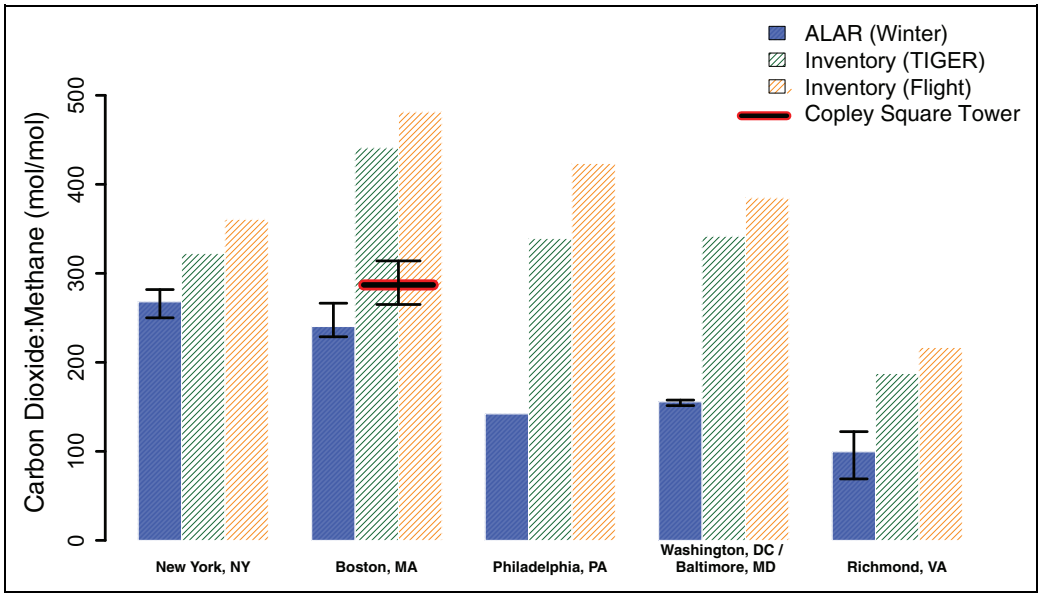

Figure 6. CO_2: CH_4 flux ratios for each urban domain sampled in the winter. Ratios measured by the aircraft (blue) are compared to ratios computed from two inventories Anthropogenic Carbon Emission System (CO_2) and GEPA (CH_4). The red line shows the ratio measured by the Copely Tower in the Harvard Urban Greenhouse Gas Network. All results are shown in $(\mathbf{moles}_{CO_2}) * (\mathbf{moles}_{CH_4})^{-1}$. DOI: https://doi.org/10.1525/elementa.2021.000119.f6

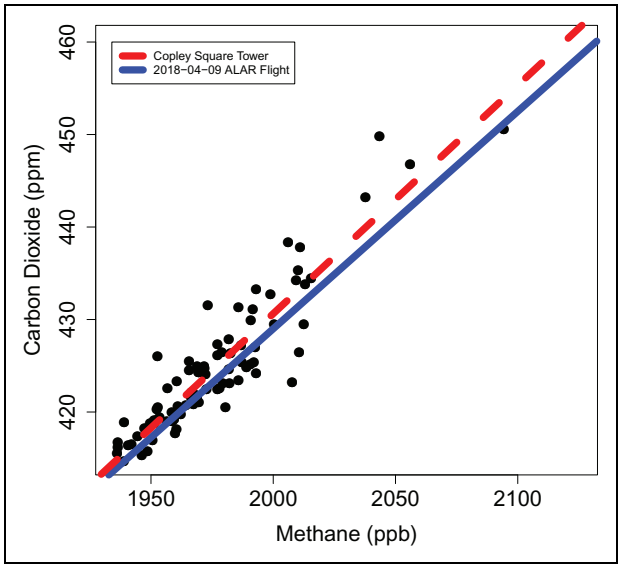

Figure 7. Comparison of aircraft flux ratios to urban tower measurements. Points are hourly mean daytime CH_4 and CO_2 measurements from Copley Tower for the month of April 2018 and are compared to the calculated CO_2: CH_4 ratio from the April 9, 2018, Flight over the Boston, MA, urban core. DOI: https://doi.org/10.1525/elementa.2021.000119.f7

To address this issue, we have combined an atmospheric transport model with the upwind observations made from the aircraft to enable us to compute an MDI and subtract background values informed by both model meteorology and aircraft observations. We can propagate the uncertainty associated with our subtracted background values when we estimate the uncertainty of our final answer. As with any method of background estimation using upwind aircraft sampling, we make assumptions as to the applicability of upwind concentrations observed to the downwind transect. In these flights, we attempted to plan flights on days when the wind direction was expected to be relatively steady throughout the domain for the duration of the sampling, and, when operational constraints allowed, we sampled the upwind transect first. As shown in **Figure 5**, the relative uncertainty of our TMER estimates is variable and a function of the uncertainty estimated in the MDI (Equation 2 and Section 3 of the SI) and fluctuations in the pipeline EMER reported for each domain in the 10 days prior to the measurement. The uncertainty of the TMER is potentially underestimated on three flights, indicated by an "*" in Figure 1 (New York, NY [March 20, 2018], Philadelphia, PA [April 26, 2018], and Indianapolis, IN [June 19, 2017]). Further analysis of the flights with added uncertainty is described in detail in Section 6 of the SI. For the September 2, 2017, sampling flight of New York, NY, the prevailing wind direction was from the east, which justified a simple background approximation based upon the homogeneous upwind marine air mixing ratios. This flight presents the lowest uncertainty in the TMER (0.815 (+0.004/−0.006; Flux CH_4 (Thermogenic))/(Flux CH_4 (Total))) as the pipeline EMER was the determining factor and was quite stable at 0.0213 (+0.004/−0.003) $molC_2H_6/molCH_4$. For the August 28, 2017, flight sampling Philadelphia, PA, there were significant CH_4 sources of biogenic origin upwind of the domain, which manifested as a larger uncertainty estimation in the bounds of the MDI and ultimately a larger uncertainty in the calculated TMER (0.384 (+1.23/−0.13) $(\frac{FluxCH_4(Thermogenic)}{FluxCH_4(Total)})$.

To compute the TMER in this study, we integrated the enhancements computed from the downwind transects (Equation 1). Previous studies have used the slopes of

tracer-tracer plots to determine similar relationships (Plant et al., 2019). We did the same for our data to compare our results to these methods. If the emissions are measured close to a city, such that the plume has not mixed homogeneously in the horizontal coordinate (e.g., if the correlation coefficient is not excellent), the slopes computed by this analysis can be significantly skewed by unmixed source plumes with high mixing ratios. This analysis is described in detail in Section 10 of the SI.

4.2. CO_2: CH_4 ratios

As shown in **Figure 6**, the observed CO_2: CH_4 ratios are all statistically significantly smaller than those from the emission model ratios. This largely reflects an underestimate of the CH_4 emissions in the GEPA inventory, consistent with the results here implying that the GEPA inventory underestimates the thermogenic CH_4 emissions, for all cities. This has been observed for other cities (Plant et al., 2019). The ACES CO_2 inventory has uncertain estimated to be $< \pm 10\%$ (Gately and Hutyra, 2017), supported by the top-down analysis of CO_2 in Boston, MA (Sargent et al., 2018), and bias in ACES is unlikely to explain the large systematic differences between observed and inventory ratios.

4.3. Defining the domain

Unambiguously defining the domain sampled during an airborne study is another difficult task when analyzing regional scale airborne measurements. Because many of the domains sampled in this study are located in the densely populated East Coast of the United States, we employed the STILT model to better describe the relative sensitivity of our TMER calculation to emissions from ground sources throughout the domain. The ground source sensitivity maps shown in **Figure 4C** and in Section 5 of the SI show the normalized spatially resolved influence of the sampling domain on the flux through the downwind transect drawn by the aircraft.

The flux sensitivity maps, in almost all cases, show that downwind concentrations are sensitive to emissions from grid boxes upwind of the domain, hence our focus on calculating a value for MDI that would enable the subtraction of the influence of those sources from the enhancement observed downwind of the urban core. The flux sensitivity maps help us to compare multiple measurement flights of the same geographic location. They graphically demonstrate that adjustments in the aircraft flight track enable us to sample a similar domain in both seasons regardless of the fact that the meteorology may be differing across flights.

Our summer flight over Indianapolis, IN, exemplifies the importance of defining the domain that influences the observed enhancements of CH_4 and C_2H_6. On June 19, 2017, the aircraft was able to obtain two downwind transects that were suitable for analysis (i.e., completely transiting through the urban plume). Of the two transects, one was composed of a much more urban fetch, sampling the core of the Indianapolis metro area, for which we computed a TMER of 0.42 (+0.04/−0.01). In the second transect, we sampled a fetch that also included a large amount of semi-rural area in the suburbs north of the downtown metro area and computed a TMER of 0.26 (+0.01/−0.01), representing relatively greater biogenic emissions. Using the flux sensitivity maps, we are able to see that the area measured by the transect with the more rural fetch measured a more analogous domain to that sampled during the winter time measurement of Indianapolis on March 16, 2018, (this is the reported value in **Figure 5**). A higher TMER value in the urban core appears typical of other cites (e.g., Boston, MA, see above). More information on this particular flight, along with the flux sensitivity maps for these transects, can be found in Section 6 of the SI.

The sampled domain must also be taken into account when comparing the results in this study to results in the literature. Lamb et al. (2016) used measurements of C_2H_6 and CH_4 made from a tower in downtown Indianapolis (INFLUX network tower 11) during February and March 2015 to determine a TMER of approximately 0.43 (43% natural gas, 48% biogenic, and 9% other). Our summer TMER computed using the urban transect, mentioned above, compared well to theirs, but our winter TMER was significantly higher (0.71 (+0.01/−0.02)). Further analysis of the flux sensitivity of the tower and sources within those footprints would be needed to more accurately compare to the Lamb et al. tower measurements.

Political boundaries typically do not define the areas that influence aircraft measurements, making it difficult to systematically compare to inventories or to studies of other cities. We have compared our results to inventories sampled using both political boundaries and the exact area encircled by the aircraft (Figures 5 and 6) and shown that the TMER of a "city" can vary significantly based on that definition. We suspect that some of this variance is driven by the presence of biogenic CH_4 point sources (landfills, WWTPs, active methanogenic wetland areas, etc.) near the upwind boundary of the urban domain. Evidently, the TMER of a city can be quite sensitive to whether these point sources influence the observations, or not. We conclude that defining the actual domain sampled in the study is crucial to interpreting top down studies of emissions and that a quantitative analysis of individual flight domains must be used when comparing measurements of a single urban area that may have been made under different meteorological conditions. We have presented here a straightforward method to make these comparisons.

4.4. Thermogenic fraction discussion

Local policy makers have shown a willingness to introduce legislation to spearhead greenhouse gas emission reductions at the city level. Local Law 97 (a component of the New York, NY, Climate Mobilization Act) is one example. It sets aggressive greenhouse gas emission reduction targets for buildings larger than 25,000 ft^2 in New York, NY, with a $268/ton fine for emissions above the target. As more cities begin to evaluate the prospect of CH_4-specific emission reduction legislation, it will be more pressing for the scientific community to inform local policy makers of the emission sectors that dominate their local CH_4 emission profile so that emission reduction strategies can address the most effective approaches. In order to make such

recommendations, we must be prepared with well-characterized CH_4 emission statistics for specific cities, which need to be supported by measurement campaigns, as current CH_4 inventories do not accurately reflect the distribution of sources and emission rates in the urban domain. New York, NY, is a good example, where we found that the overwhelming majority of CH_4 emissions are derived from natural gas sources, an observation that is not consistent with the distribution of sources in the GEPA inventory.

In this study, we have partitioned CH_4 emissions between biogenic and thermogenic sources for seven major urban areas. As shown in **Figure 5**, the GEPA CH_4 emission inventory currently underestimates the natural gas contribution to CH_4 emissions, in some cases (New York, NY, Boston, MA, Chicago, IL) by as much as 50%.

Our results showed statistically significant seasonality in the urban TMER in four of the six cities we were able to sample in both winter and summer. But CH_4 emission inventories still lack adequate seasonal resolution, making it impossible to accurately assess temporally varying emissions from data. We note that the significant biogenic sources in most urban environments are sewer systems, landfills, and wastewater treatment facilities and that there is likely some significant seasonality in those emissions not captured in the emission models (Cambaliza et al., 2014; Fries et al., 2018). Based on what is known about the seasonality of biogenic CH_4 sources and the seasonally invariant thermogenic emissions observed by Mckain et al., we suspect that biogenic emissions are the source of the seasonality in the urban TMER. Further research is needed to quantify the seasonal amplitude of the CH_4 flux from specific biogenic sectors and sources. Furthermore, recent studies have suggested that the total inventory flux estimates from many of the same urban areas measured in this analysis underestimate total emissions (McKain et al., 2015; Plant et al., 2019).

The results from our study illustrate how dramatically different the CH_4 emission profiles can be from city to city. We find the TMER varying as much as a factor of 3 (0.32 for Richmond, VA, to 1.0 for New York, NY, in winter months). These differences can occur for multiple reasons. Cities with older natural gas infrastructure (e.g., with cast iron NG mains) such as New York, NY, and Boston, MA, can have greater natural gas emissions (Von Fischer et al., 2017). Some cities, such as Boston, MA, do not have landfills in the urban core where some, such as Richmond, have multiple. Future studies should aim to quantify both the TMER and total CH_4 flux from a larger distribution of cities to better quantify the emissions from cities with a wide array of potential source infrastructure.

5. Conclusion

Current emission inventories for the United States significantly underestimate the role of natural gas relative to biogenic CH_4 emissions in urban environments. Local policy makers must have knowledge of the emission profile of their city in order to best allocate resources and introduce and implement legislation to reduce greenhouse gas emissions. Our work suggests that urban areas with significant landfill infrastructure (e.g., Richmond, VA) may benefit from better landfill gas capture and recovery systems, whereas urban areas with dense and aging natural gas infrastructure (e.g., Boston, MA, and New York, NY) should devote their resources toward updating their natural gas distribution infrastructure and possibly controlling post-meter emissions. Our results also highlight the need for more urban scale observational CH_4 data in order to better parameterize the emission accounting used in national level CH_4 emission inventories. Currently, inventories are unable to provide the comprehensive bottom-up picture that they were designed to provide, and improvements require higher quality flux estimates from urban CH_4 sources, combining top-down and bottom-up methodologies.

Data accessibility statement

Flight data are available to the public and can be accessed from the Harvard Dataverse at https://doi.org/10.7910/DVN/T7ANQD.

Supplemental files

The supplemental files for this article can be found as follows: See attached Supplementary Materials.

Acknowledgments

We would like to thank our colleagues Israel Lopez-Coto and Anna Karion for their support and guidance with respect to our mission planning and deployment. We also acknowledge Eric Kort and Genevieve Plant at the University of Michigan for their contribution to the NOAA ECO campaign which in turn led to us being able to use those data. Perhaps most importantly, we acknowledge the fine support of the aircraft operations folks at Purdue University whose diligent work gave us confidence that every time ALAR took off, it would return home safe and allow us to bring data along with it.

Funding

We thank the National Institute of Standards and Technology (NIST) for partial support of this work, via Award No. 70NANB16H262. Certain commercial equipment, instruments, or materials are identified in this article in order to specify the experimental procedure adequately. Such identification is not intended to imply recommendation or endorsement by NIST nor is it intended to imply that the materials or equipment identified is necessarily the best available for the purpose.

Competing interests

The authors declare no competing interest. Paul B. Shepson is an Associate Editor at *Elementa*. He was not involved in the review process of this article.

Author contributions

Contributed to the acquisition of the data: CF, PBS, BHS, KH.

Contributed to the analysis of the data: CF, KH, SW.

Contributed to the development of the ethane analyzer: CF, BD, SW.

Contributed data from the NOAA ECO campaign for the winter Philadelphia Flight: CS.

References

Alvarez, RA, Alvarez, RA, Zavala-Araiza, D, Lyon, DR, Allen, DT, Barkley, ZR, Brandt, AR, Davis, KJ, Herndon, SC, Jacob, DJ, Karion, A, Kort, EA, Lamb, BK, Lauvaux, T, Maasakkers, JD, Marchese, AJ, Omara, M, Pacala, SW, Peischl, J, Robinson, AL, Shepson, PB, Sweeney, C, Townsend-Small, A, Wofsy, SC, Hamburg, SP. 2018. Assessment of methane emissions from the U.S. oil and gas supply chain. *Science* **361**(6398): 186–188. DOI: http://dx.doi.org/10.1126/science.aar7204.

Bares, R, Lin, JC, Hoch, SW, Baasandorj, M, Mendoza, DL, Fasoli, B, Mitchell, L, Catharine, D, Stephens, BB. 2018. The wintertime covariation of CO_2 and criteria pollutants in an urban valley of the Western United States. *Journal of Geophysical Research: Atmospheres* **123**(5): 2684–2703. DOI: http://dx.doi.org/10.1002/2017JD027917.

Börjesson, G, Svensson, BH. 1997. Seasonal and diurnal methane emissions from a landfill and their regulation by methane oxidation. *Waste Management and Research* **15**(1): 33–54. DOI: http://dx.doi.org/10.1006/wmre.1996.0063.

Briber, B, Hutyra, L, Dunn, A, Raciti, S, Munger, J. 2013. Variations in atmospheric CO_2 mixing ratios across a Boston, MA Urban to Rural Gradient. *Land* **2**(3): 304–327. DOI: http://dx.doi.org/10.3390/land2030304.

Cambaliza, MO, Shepson, PB, Caulton, DR, Stirm, B, Samarov, D, Gurney, KR, Turnbull, J, Davis, KJ, Possolo, A, Karion, A, Sweeney, C, Moser, B, Hendricks, A, Lauvaux, T, Mays, K, Whetstone, J, Huang, J, Razlivanov, I, Miles, NL, Richardson, SJ. 2014. Assessment of uncertainties of an aircraft-based mass balance approach for quantifying urban greenhouse gas emissions. *Atmospheric Chemistry and Physics* **14**(17): 9029–9050. DOI: http://dx.doi.org/10.5194/acp-14-9029-2014.

Crawford, TL, Dobosy, RJ. 1992. A sensitive fast-response probe to measure turbulence and heat flux from any airplane. *Boundary-Layer Meteorology* **59**(3): 257–278. DOI: http://dx.doi.org/10.1007/BF00119816.

Crosson, ER. 2008. A cavity ring-down analyzer for measuring atmospheric levels of methane, carbon dioxide, and water vapor. *Applied Physics B: Lasers and Optics* **92**(Special Issue 3): 403–408. DOI: http://dx.doi.org/10.1007/s00340-008-3135-y.

Cui, YY, Brioude, J, McKeen, SA, Angevine, WM, Kim, S-W, Frost, GJ, Ahmadov, R, Peischl, J, Bousserez, N, Liu, Z, Ryerson, TB, Wofsy, SC, Santoni, GW, Kort, EA, Fischer, ML, Trainer, M. 2015. Top-down estimate of methane emissions in California using a mesoscale inverse modeling technique: The South Coast Air Basin. *Journal of Geophysical Research: Atmospheres* **120**(13): 6698–6711. DOI: http://dx.doi.org/10.1002/2014JD023002.

Eilerman, S, Peischl, J, Neuman, J, Ryerson, T, Aikin, K, Holloway, MW, Zondlo, MA, Golston, LM, Pan, D, Floerchinger, C, Herndon, S. 2016. Characterization of ammonia, methane, and nitrous oxide emissions from concentrated animal feeding operations in northeastern Colorado. *Environmental Science and Technology* **50**(20): 10885–10893. DOI: http://dx.doi.org/10.1021/acs.est.6b02851.

Fasoli, B, Bowling, DR, Mitchell, L, Mendoza, D, Lin, JC. 2018. Simulating atmospheric tracer concentrations for spatially distributed receptors: Updates to the Stochastic Time-Inverted Lagrangian Transport model's R interface (STILT-R version 2). *Geoscientific Model Development* **11**(7): 2813–2824. DOI: http://dx.doi.org/10.5194/gmd-11-2813-2018.

Fries, AE, Schifman, LA, Shuster, WD, Townsend-small, A. 2018. Street-level emissions of methane and nitrous oxide from the wastewater collection system in Cincinnati, Ohio. *Environmental Pollution* **236**: 247–256. DOI: http://dx.doi.org/10.1016/j.envpol.2018.01.076.

Garman, KE, Hill, KA, Wyss, P, Carlsen, M, Zimmerman, JR, Stirm, BH, Carney, TQ, Santini, R, Shepson, PB. 2006. An airborne and wind tunnel evaluation of a wind turbulence measurement system for aircraft-based flux measurements. *Journal of Atmospheric and Oceanic Technology* **23**(12): 1696–1708. DOI: http://dx.doi.org/10.1175/JTECH1940.1.

Gately, CK, Hutyra, LR. 2017. Large uncertainties in urban-scale carbon emissions. *Journal of Geophysical Research: Atmospheres* **122**(20): 242–260. DOI: http://dx.doi.org/10.1002/2017JD027359.

Gerbig, C, Körner, S, Lin, JC. 2008. Vertical mixing in atmospheric tracer transport models: Error characterization and propagation. *Atmospheric Chemistry and Physics* **8**(3): 591–602.

Heimburger, AMF, Harvey, RM, Shepson, PB, Stirm, BH, Gore, C, Turnbull, J, Cambaliza, MOL, Salmon, OE, Kerlo, A-EM, Lavoie, TN, Davis, KJ, Lauvaux, T, Karion, A, Sweeney, C, Brewer, WA, Hardesty, RM, Gurney, KR. 2017. Assessing the optimized precision of the aircraft mass balance method for measurement of urban greenhouse gas emission rates through averaging. *Elementa: Science of the Anthropocene* **5**: 26. DOI: http://dx.doi.org/10.1525/elementa.134.

Karion, A, Sweeney, C, Kort, EA, Shepson, PB, Brewer, A, Cambaliza, M, Conley, SA, Davis, K, Deng, A, Hardesty, M, Herndon, SC, Lauvaux, T, Lavoie, T, Lyon, D, Newberger, T, Pétron, G, Rella, C, Smith, M, Wolter, S, Yacovitch, TI, Tans, P. 2015. Aircraft-based estimate of total methane emissions from the Barnett Shale Region. *Environmental Science and Technology* **49**(13): 8124–8131. DOI: http://dx.doi.org/10.1021/acs.est.5b00217.

Kidnay, AJ, Parrish, WR, McCartney, DG. 2011. *Fundamentals of natural gas processing*. DOI: http://dx.doi.org/10.1201/b14397.

Lamb, BK, Cambaliza, MO, Davis, KJ, Edburg, SL, Ferrara, TW, Floerchinger, C, Heimburger, AMF, Herndon, S, Lauvaux, T, Lavoie, T, Lyon, DR,

Miles, N, Prasad, KR, Richardson, S, Roscioli, JR, Salmon, OE, Shepson, PB, Stirm, BH, Whetstone, J. 2016. Direct and indirect measurements and modeling of methane emissions in Indianapolis, Indiana. *Environmental Science and Technology* **50**(16): 8910–8917. DOI: http://dx.doi.org/10.1021/acs.est.6b01198.

Lin, JC, Gerbig, C. 2005. Accounting for the effect of transport errors on tracer inversions. *Geophysical Research Letters* **32**(1): 1–5. DOI: http://dx.doi.org/10.1029/2004GL021127.

Lin, JC, Gerbig, C, Wofsy, SC, Andrews, AE, Daube, BC, Davis, KJ, Grainger, CA. 2003. A near-field tool for simulating the upstream influence of atmospheric observations: The Stochastic Time-Inverted Lagrangian Transport (STILT) model. *Journal of Geophysical Research: Atmospheres* **108**. DOI: http://dx.doi.org/10.1029/2002JD003161.

Maasakkers, JD, Jacob, DJ, Sulprizio, MP, Turner, AJ, Weitz, M, Wirth, T, Hight, C, DeFigueiredo, M, Desai, M, Schmeltz, R, Hockstad, L, Bloom, AA, Bowman, KW, Jeong, S, Fischer, ML. 2016. Gridded national inventory of U.S. methane emissions. *Environmental Science and Technology* **50**(23). DOI: http://dx.doi.org/10.1021/acs.est.6b02878.

Marchese, AJ, Vaughn, TL, Zimmerle, DJ, Martinez, DM, Williams, LL, Robinson, AL, Mitchell, AL, Subramanian, R, Tkacik, DS, Roscioli, JR, Herndon, SC. 2015. Methane emissions from United States natural gas gathering and processing. *Environmental Science and Technology* **49**(17): 10718–10727. DOI: http://dx.doi.org/10.1021/acs.est.5b02275.

McKain, K, Down, A, Raciti, SM, Budney, J, Hutyra, LR, Floerchinger, C, Herndon, SC, Nehrkorn, T, Zahniser, MS, Jackson, RB, Phillips, N, Wofsy, SC. 2015. Methane emissions from natural gas infrastructure and use in the urban region of Boston, Massachusetts. *Proceedings of the National Academy of Sciences* **112**(7): 1941–1946. DOI: http://dx.doi.org/10.1073/pnas.1416261112.

Merrin, Z, Francisco, PW. 2019. Unburned methane emissions from residential natural gas appliances. *Environmental Science and Technology* **53**(9): 5473–5482. DOI: http://dx.doi.org/10.1021/acs.est.8b05323.

Plant, G, Kort, E, Floerchinger, C, Gvakharia, A, Vimont, I, Sweeney, C. 2019. Large fugitive methane emissions from urban centers along the US East Coast. *Geophysical Research Letters* **46**(14): 8500–8507. DOI: http://dx.doi.org/10.1029/2019GL082635.

Roscioli, JR, Yacovitch, TI, Floerchinger, C, Mitchell, AL, Tkacik, DS, Subramanian, R, Martinez, DM, Vaughn, TL, Williams, L, Zimmerle, D, Robinson, AL, Herndon, SC, Marchese, AJ. 2015. Measurements of methane emissions from natural gas gathering facilities and processing plants: Measurement methods. *Atmospheric Measurement Techniques* **8**(5): 2017–2035. DOI: http://dx.doi.org/10.5194/amt-8-2017-2015.

Saint-Vincent, PM, Pekney, NJ. 2020. Beyond-the-meter: Unaccounted sources of methane emissions in the natural gas distribution sector. *Environmental Science and Technology* **54**(1): 39–49. DOI: http://dx.doi.org/10.1021/acs.est.9b04657.

Sargent, M, Barrera, Y, Nehrkorn, T, Hutyra, LR, Gately, CK, Jones, T, McKain, K, Sweeney, C, Hegarty, J, Hardiman, B, Wofsy, SC. 2018. Anthropogenic and biogenic CO_2 fluxes in the Boston urban region. *Proceedings of the National Academy of Sciences* **115**(40): E9507–E9507. DOI: http://dx.doi.org/10.1073/pnas.1815348115.

Smith, ML, Kort, EA, Karion, A, Sweeney, C, Herndon, SC, Yacovitch, TI. 2015. Airborne ethane observations in the Barnett Shale: Quantification of ethane flux and attribution of methane emissions. *Environmental Science & Technology*. 49(13):8158–8166. DOI: http://dx.doi.org/10.1021/acs.est.5b00219.

Stein, AF, Draxler, RR, Rolph, GD, Stunder, BJ, Cohen, MD, Ngan, F. 2015. Noaa's HYSPLIT atmospheric transport and dispersion modeling system. *Bulletin of the American Meteorological Society* **96**(12): 2059–2077. DOI: http://dx.doi.org/10.1175/BAMS-D-14-00110.1.

Subramanian, R, Williams, L, Vaughn, T, Zimmerle, D, Roscioli, J, Herndon, SC, Yacovitch, TI, Floerchinger, C, Tkacik, DS, Mitchell, AL, Sullivan, MR, Dallmann, TR, Robinson, AL. 2015. Methane emissions from natural gas compressor stations in the transmission and storage sector: Measurements and comparisons with the EPA greenhouse gas reporting program protocol. *Environmental Science and Technology* **49**(5): 3252–3261. DOI: http://dx.doi.org/10.1021/es5060258.

Von Fischer, JC, Cooley, D, Chamberlain, S, Gaylord, A, Griebenow, CJ, Hamburg, SP, Salo, J, Schumacher, R, Theobald, D, Ham, J. 2017. Rapid, vehicle-based identification of location and magnitude of urban natural gas pipeline leaks. *Environmental Science and Technology* **51**(7): 4091–4099. DOI: http://dx.doi.org/10.1021/acs.est.6b06095.

Yacovitch, TI, Herndon, SC, Roscioli, JR, Floerchinger, C, McGovern, RM, Agnese, M, Pétron, G, Kofler, J, Sweeney, C, Karion, A, Conley, SA, Kort, EA, Nähle, L, Fischer, M, Hildebrandt, L, Koeth, J, McManus, JB, Nelson, DD, Zahniser, MS, Kolb, CE. 2014. Demonstration of an ethane spectrometer for methane source identification. *Environmental Science and Technology* **48**(14): 8028–8034. DOI: http://dx.doi.org/10.1021/es501475q.

How to cite this article: Floerchinger, C, Shepson, PB, Hajny, K, Daube, BC, Stirm, BH, Sweeney, C, Wofsy, SC. 2021. Relative flux measurements of biogenic and natural gas-derived methane for seven U.S. cities. *Elementa Science of the Anthropocene* 9(1). DOI: https://doi.org/10.1525/elementa.2021.000119.

Domain Editor-in-Chief: Detlev Helmig, Boulder A.I.R. LLC, Boulder, CO, USA

Associate Editor: Isobel Jane Simpson, Department of Chemistry, University of California, Irvine, CA, USA

Knowledge Domain: Atmospheric Science

Published: February 18, 2021 **Accepted:** December 20, 2020 **Submitted:** August 13, 2020

ELEMENTA Science of the Anthropocene

Elem Sci Anth is a peer-reviewed open access journal published by University of California Press.

OPEN ACCESS